Crystal Plasticity Analysis of Change in Incompatibility and Activities of Slip Systems in α-phase of Ti alloy under Cyclic Loading

Yoshiki Kawano[1,a*], Tetsuya Ohashi[1,b], Tsuyoshi Mayama[2,c], Ryoji Kondou [3,d]

[1]Department of Mechanical Engineering, Kitami Institute of Technology, Kitami 090-8507, Japan

[2]Department of Materials Science and Engineering, Kumamoto University, Kumamoto 860-8555, Japan

[3]Faculty of Engineering Department of Mechanical Systems Engineering, University of the Ryukyus, Okinawa 903-0213, Japan

[a]kawano_y@mail.kitami-it.ac.jp, [b]ohashi@newton.mech.kimati-it.ac.jp,

[c]mayama@kumamoto-u.ac.jp, [d]kondou@teada.tec.u-ryukyu.ac.jp,

Highlights

- Changes in activities of slip systems in the α-phase of Ti-6Al-4V under cyclic loading are investigated by crystal plasticity analysis of bicrystals.
- The trade-off relationship of activities of the basal slip system is observed in a crystal grain and the prismatic <a> slip system in the other crystal grains.
- Incompatibility between the crystal grains due to elastic anisotropy and its changes by work hardening exhibits the potential to lead the trade-off relationship.
- The mechanisms of the trade-off relationship are more easily explained by wedge disclination type deformation fields.

Abstract

With respect to Ti-6Al-4V alloy (Ti-64) with duplex phases constructed by α-phase with an hcp structure and β-phase with a bcc structure, basal slips in α-phase can potentially lead to crack initiation under fatigue loading. Hence, it is necessary to quantitatively evaluate the activity of basal slip systems. However, the critical resolved shear stress (CRSS) for the basal slips in α-phase is equal to or slightly exceeds that for the prismatic slips, and mechanisms for the activation of slip systems are not completely understood. The present study involved conducting crystal plasticity analysis of α-phase subjected to cyclic loading and uniaxial tensile loading employing bicrystal models and uniaxial tensile analysis of tricrystal models. The results indicated that a trade-off relationship exists between the activities of slip systems. Specifically, the inactivation of prismatic <a> slip system in a crystal grain activates the basal slip system in the neighboring crystal grains due to the changes of incompatibility by work hardening around the boundary triple junction line. The changes in incompatibility can be explained by wedge disclination type deformation field.

Keywords: Crystal plasticity analysis, Activities of slip systems, α-phase, Cyclic loading, incompatibility

1. Introduction

Ti alloys are widely used in several fields, including aerospace, medical, and sports. Thus, improvements in the accuracy of the fatigue life predictions are important. Specifically, Ti-6Al-4V (Ti-64) is the most widely used Ti alloy [1], and the enhancement in the quality of predictions can lead to developments of products with higher reliability and performance. However, the fatigue mechanisms of Ti-64 are not fully understood.

Ti-64 with duplex phases is composed of α-phase with an hcp structure and β-phase with a bcc structure. The microstructures of Ti-64 change due to plastic forming and heat treatments [1,2] and include fully lamellar microstructures, equiaxed microstructures, and bimodal type microstructures. When a globular α-phase (primary α) exists in the microstructures, fatigue crack initiation is mainly observed within the basal slip bands in the primary α [3,4]. This suggests the high activity of the basal slip system, and the basal slips influence the fatigue failure in the primary stage [4-6].

Under fatigue loadings, the number of cycles required to nucleate a crack may constitute 5-20% of the total lifetime in the high cycle fatigue (HCF) regime [7,8] and higher percentages in the very high cycle fatigue (VHCF) when compared with those of HCF [8]. Thus, it is necessary to quantitatively evaluate the activity of a basal slip system to reveal initial fatigue mechanisms in Ti-64.

Active slip systems of primary α in Ti-64 are basal slip system, prismatic <a> slip system, first-order pyramidal <a> slip system, and first-order pyramidal <c+a> slip system [9,10].

The basal and prismatic <a> are mainly observed as active slip systems in Ti-64 under fatigue loadings. However, previous studies [9,11-13] showed that critical resolved shear stress (CRSS) on the basal slip system is equal to or slightly exceeds that for the prismatic <a> slip system. Thus, mechanisms exist to actively operate the basal slip system. The reasons for the high activity of basal slip system remain less well-defined while other effects, such as elastic anisotropy [5] and work softening [9], can be considered as plausible reasons.

Incompatibility between crystal grains [14,15] potentially causes the high activity of a basal slip system under fatigue loadings. A reason for the incompatibility corresponds to the anisotropic elasto-plasticity in the level of crystal grains. In the deformation of polycrystals, crystal grains with anisotropic elasto-plasticity deform in different shapes from others to reflect their crystal orientations. However, their deformations are mutually constrained by the grain boundaries, and the stresses and strains become inhomogeneous. Under cyclic loadings, inactivation of slip systems by work hardening also affects incompatibility. The work hardening rates of α-Ti alloy change based on interstitial elements such as oxygen [16]. Thus, it is important to reveal the mechanisms of fatigue failure in the primary stage to understand the relationship between changes of incompatibility and activities of slip systems.

Mechanical interactions between crystal grains in polycrystals are considerably complex, and analysis employing bicrystals were performed to obtain simpler understandable results. Previous studies indicated that localized stresses occurred near the grain boundaries due to the incompatibility, and the stresses inhibit or enhance the activities of

slip systems [17,18]. Specifically, reports suggest that crack initiation occurs in the regions far from the grain boundary of bicrystals with high compatibility while cracks nucleate from the grain boundary of bicrystals with incompatibility [14]. However, results obtained even by the analysis employing bicrystals are complex, and cannot not be easily understood only by experimental methods. Thus, numerical analysis of bicrystals has been conducted by molecular dynamics (MD) [19,20], finite element method (FEM) [21,22]. Furthermore, FEM analyses dealing with continuum cannot track the behavior of dislocations on an atomic scale but can reproduce interactions between them in the crystal grain scale.

Extant studies performed the analysis of bicrystals by employing crystal plasticity finite element methods (CPFEM). The effects of elasticity and plasticity are considered separately by CPFEM. Ohashi [21] performed uniaxial tensile analysis of a plastically incompatible type bicrystal in which crystal grains were arranged in the loading direction and reproduced inhomogeneous deformation near the grain boundary. Kondou & Ohashi [23] performed uniaxial tensile analysis of a compatible type bicrystal in which crystal grains were arranged in a direction perpendicular to the loading direction. The results indicated that the bicrystal was inhomogeneously deformed by the effect of changes in the shapes of grains due to plastic anisotropy and the displacement constraints and that dislocation bands were formed by the inhomogeneous deformation. Mayama et al. [24] conducted a cyclic loading plasticity analysis employing a bicrystal model similar to that used by Kondou & Ohashi [23], and investigated the relationship between the dislocation patterns and amplitudes of strains. Kawano et al. [25] investigated the relationship between inhomogeneous deformations and changes in incompatibility due to inclinations

of the grain boundary in bicrystal models. However, there is a paucity of studies examining anisotropic elasticity with respect to changes in incompatibility under cyclic loadings.

The fore-mentioned studies show that the combination of changes in shapes of crystal grains by plastic deformations and the boundary conditions induce inhomogeneous deformation even in compatible-type bicrystals in which crystal grains are arranged in a direction perpendicular to the loading direction. In contrast, interactions do not occur between crystal grains by plastic deformation when the angles of slip plane normal vectors and slip directions correspond to 45º in the loading direction and plastic strains in the loading direction are equal between the crystal grains. This is because the shearing components of plastic deformations correspond to zero under the conditions (as shown in Fig. 1).

As previously stated, crystal plasticity analysis employing bicrystals simplifies the phenomena and aids in understanding the results. However, it is necessary to focus on the difference in the displacement constraints between bicrystals and actual materials. With respect to the above analysis employing bicrystals, displacement constraints exist on the bottom surfaces, and uniform displacements are applied to the top surfaces. Thus, the shapes of bottom and top surfaces remain flat throughout the deformation process independent of nonuniformity and anisotropy in the materials. The constraint surfaces are considered as the constraint due to “pseudo” crystal grains [26]. However, the constraint condition is strict when compared to the actual condition. Crystal grains in structural materials commonly deform without maintaining the flat shapes of grain boundaries. It is

necessary to investigate the effects of the constraint conditions on the results.

In this study, crystal plasticity analysis of α-phase is performed to reveal the effects of elastic anisotropy and work hardening on the activity of basal slip system by employing bi- and tricrystal models. First, cyclic loading analysis using a bicrystal model is performed to survey the activity changes in basal and prismatic <a> slip systems. Second, the reasons for the activity changes are investigated by using analyses employing bicrystal and tricrystal models. The effects of boundary conditions of bicrystal models on the activities of slip systems are also investigated using tricrystal models.

2. Procedure for crystal plasticity analysis

2.1 Constitutive equations

A three-dimensional crystal plasticity finite element analysis code developed by Ohashi [21,23-27] was employed. The constitutive equations employed in the study are shown below. It is assumed that Schmid's law is used, and an elasto-plastic constitutive equation for slip deformation is given as follows:

$$\dot{\varepsilon}_{ij} = \left[S^{e}_{ijkl} + \sum_{n} \sum_{m} \left\{ h^{(nm)} \right\}^{-1} P^{(n)}_{ij} P^{(m)}_{kl} \right] \dot{\sigma}_{kl} , \tag{1}$$

where $\dot{\varepsilon}_{ij}$, $\dot{\sigma}_{kl}$, S^{e}_{ijkl}, $h^{(nm)}$ and $P^{(n)}_{ij}$ denote the increment in the strain, the increment in the Cauchy's stress tensor, elastic compliance, coefficient of work hardening, and the Schmid tensor, respectively [28]. The superscripts *m* and *n* indicate slip systems. The CRSS is given by a modified Bailey-Hirsch model as follows:

$$\theta^{(n)} = \theta_0(T) + \sum_{m} a \mu \tilde{b} \Omega^{(nm)} \sqrt{\rho^{(m)}_S} , \tag{2}$$

where θ_0, $\Omega^{(nm)}$, a, μ, $\tilde{b}$ and $\rho^{(m)}_S$ denote the lattice friction stress, interaction matrix between slip systems, a numerical factor of the order of 0.1, elastic shear modulus, magnitude of Burgers vector, and density of statistically stored dislocations (SSDs), respectively [27]. The increment in the SSD density is given as follows:

$$\dot{\rho}^{(n)}_S = \frac{c \dot{\gamma}^{(n)}}{\tilde{b} L^{(n)}} , \tag{3}$$

where c is a numerical coefficient of the order of 1 and $\dot{\gamma}^{(n)}$ denotes the increment in the plastic strain. Additionally, $L^{(n)}$ is the mean free path of dislocations that is defined as follows:

$$L^{(m)} = \frac{c^*}{\sqrt{\sum_k \omega^{(km)} (\rho_S^{(k)} + \left\| \rho_G^{(k)} \right\|)}}, \tag{4}$$

where c^* and $\omega^{(km)}$ denote a numerical constant and the weight matrix. $\left\| \rho_G^{(k)} \right\|$ is the norm of geometrically necessary dislocation (GND) density defined as follows:

$$\left\| \rho_G^{(m)} \right\| = \sqrt{(\rho_{G,edge}^{(m)})^2 + (\rho_{G,screw}^{(m)})^2}, \tag{5}$$

$$\rho_{G,edge}^{(m)} = -\frac{1}{\tilde{b}} \frac{\partial \gamma^{(m)}}{\partial \xi^{(m)}}, \quad \rho_{G,screw}^{(m)} = \frac{1}{\tilde{b}} \frac{\partial \gamma^{(m)}}{\partial \zeta^{(m)}}, \tag{6}$$

where $\rho_{G,edge}^{(m)}$ and $\rho_{G,screw}^{(m)}$ are densities of edge and screw components of GNDs, respectively. Here $\xi^{(m)}$ and $\zeta^{(m)}$ denote directions parallel and perpendicular to the slip direction on the slip plane, respectively. The increment of the CRSS is given as follows:

$$\dot{\theta}^{(n)} = h^{(nm)} \dot{\gamma}^{(m)}. \tag{7}$$

The strain hardening coefficient $h^{(nm)}$ is obtained from Eqs. 2-4 and Eq. 7 as follows:

$$h^{(nm)} = \frac{ac\mu\Omega^{(nm)}}{2L^{(m)}\sqrt{\rho_S^{(m)}}}. \tag{8}$$

When GN dislocations accumulate in materials under cyclic loading, internal stress field will develop and this will affect the subsequent activities of dislocations and result in the Bauschinger effect under cyclic loading. Recently, this effect of internal stress is being introduced in cyclic loading analyses [29]. However, the full understandings of GN dislocations near grain boundaries as a source of back stress are still controversial. Thus, the effect of internal stress is not taken into account in the current study although the

higher-order theory [30] is one possibility.

2.2 Finite element analysis models

2.2.1 Bicrystal model

Crystal plasticity analysis for bicrystals is conducted with changing loading conditions, crystal orientations, and CRSSs. The geometries are shown in Figs. 2 and 3. Two types of loading conditions are employed, namely a cyclic loading condition (Fig. 2) and a uniaxial tensile loading condition (Fig. 3). The tensile or compressive loading is given by the enforced displacement in the Y-direction of all the nodes on the top surface. Additionally, all the nodes on the bottom surface are fixed in the Y-direction. Elastic compliances for Ti with a hcp structure employed in the analyses are described in Table 1 [31].

The cyclic loading analysis (Fig. 2) is conducted employing four sets of c^* shown in Table 2. Work hardening rates increase with decreases in c^* since the mean free path of moving dislocations becomes shorter and accumulation rates of SSDs increase on the condition of higher c^*. In Table 2, EQ-hardening is the condition in which work hardening rates are identical between basal and prismatic <a> slip systems, and No-basal hardening is the condition in which work hardening does not occur on the basal slip system.

In α-phase in Ti-64, relative CRSSs for the prismatic <a> slip system normalized to CRSS for the basal slips correspond to 0.93-1.30 as reported by Medina Perilla & Gil Sevillano [11], 1.43 by Seminatin & Beiler [12], and 1.135 by Bridier et al. [9]. Gil Sevillano [11] experimentally estimated that the CRSSs for the basal and prismatic <a> slip systems

correspond to 395 MPa and approximately 500 MPa, respectively. Bridier et al. [13] estimated 420MPa for the basal slips and 370 MPa for the prismatic <a> slips by the data from Bridier et al. [9]. In the PRI-BSL cyclic analysis (Fig. 2) as shown in Table 3, 425.5 MPa and 370 MPa are employed as the CRSSs for the basal slips and prismatic <a> slips, respectively. The relative CRSS of the basal slip system normalized to the CRSS for the prismatic <a> slips corresponds to 1.15. The crystal orientations are set such that the prismatic <a> and basal slip systems are the primary slip systems in Grains 1 and 2, respectively.

The uniaxial tensile analysis is conducted with two types of crystal orientations, namely PRI-BSL (Fig. 3 (a)) and PRI-PRI (Fig. 3 (b)). In the PRI-PRI model, both c-axes of crystal grains correspond to the Z-axis, and prismatic <a> constitutes the primary slip system in both Grains 1 and 2. Crystal grains with the hcp structure exhibit anisotropic elasticity albeit with isotropic elasticity within the basal plane. An analysis of PRI-PRI tension is performed to compare the results of PRI-BSL analysis. In order to investigate the relationship between activities of slip systems and CRSSs, analyses are conducted several times with changing sets of CRSSs as shown in Tables 3 and 4. Several CRSSs are employed for the prismatic <a> slip system while CRSS for the basal slip system is fixed.

2.2.2 Tricrystal model

A tricrystal plasticity analysis is conducted to investigate effects of the forced displacement on the bicrystal models, and the geometries are shown in Fig. 4. The tricrystal models are structured by adding the third crystal grain on the top (Fig. 4 (a)) or

bottom of the bicrystal model (Fig. 4 (b)). The boundary conditions are the same as those used in the bicrystal models. The bottom surface is fixed in the Y-direction, and the top surface is subjected to forced tensile displacement. Crystal orientations in Grains 1 and 2 are identical to those in the PRI-BSL model (Fig. 3 (a)), and it is assumed that the c-axis in Grain 3 corresponds to the loading direction. The elastic deformation in α-phase is the most difficult in the c-axis direction [32] and the Schmid factors on the basal and prismatic <a> slip systems correspond to zero in the crystal orientation of Grain 3. Thus, Grain 3 exhibits the most difficult orientation in the loading direction.

3. Results and discussion

3.1 Cyclic loading analysis

Fig. 5 shows the distributions of slip strains on the basal and prismatic <a> slip systems at the peak of tension ($\bar{\varepsilon}_{yy}$ = 0.7 %) and compression ($\bar{\varepsilon}_{yy}$ = 0.7 %) under the No-basal hardening condition with $C^*_{prismatic<a>}$=15.0. First, distributions of slip strains at the 1st cycle are observed. Slip systems operate within the regions near the corner at the bottom of the bicrystal and the grain boundary near the top surface. Schmid factors correspond to 0.5 in both Grains 1 and 2, and the primary slip systems correspond to the prismatic <a> and basal slip systems in Grain 1 and Grain 2, respectively. The active slip systems correspond to prismatic <a> system in Grain 1 and basal slip system in Grain 2. Thus, the basal slip system is activated despite CRSS for the basal slip system is higher than that of prismatic <a> slip system. This is because the α-phase is difficult to deform in the c-axis, and crystal grains with the c-axis more close to the loading direction tend to receive higher stresses [32].

Fig. 6 shows distributions of stresses in the elastic stage. The stresses are higher in Grain 2 when compared to that in Grain 1. A stress concentration is observed near the grain boundary in Grain 2. Kondou & Ohashi [33] conducted uniaxial tensile analysis employing fcc bicrystal models with tilt angle grain boundary and isotropic elasticity. The results showed that inhomogeneous deformation occurred due to plastic anisotropy and restraint of displacement on the top and bottom surfaces of the bicrystal. Additionally, the distributions of slip strains are similar to those obtained by the current study. However, a

difference also exists between the results. The current results show slip systems activated along the grain boundary in Grain 2 due to the stress concentration caused by the anisotropic elasticity. In contrast, a similar activation of slip system along the grain boundary was not observed in the study by Kondou & Ohashi [33] since the isotropic elasticity model was employed. Kondou & Ohashi [36] conducted a uniaxial tensile loading analysis of a bicrystal with anisotropic elasticity, and the results indicated that slip systems were activated along the grain boundary.

Second, changes in the distributions of slip strains are described below (Fig. 5). The slip strains are positive at the peak of tension ($\bar{\varepsilon}_{yy}$ = 0.7%) and negative in the compression ($\bar{\varepsilon}_{yy}$ = -0.7%) in the early stage of cyclic loading. The distributions of the absolute values of slip strains at the tension and compression are almost identical. In Grain 1, work hardening occurs during cyclic loading. Furthermore, the maximum slip strain decreases and positive and negative residual strains increase with cycles progress. Conversely, basal slip strains in Grain 2 exhibit a slightly increase at the corner of the bottom of the bicrystal. Other results obtained in the No-basal hardening condition with different $c^*_{prismatic<a>}$ also indicate the same tendency. Fig. 7 shows dependency of $c^*_{prismatic<a>}$ on the distributions of slip strains at the peak of tension in the 25th cycle. The above tendency is observed in the No-basal hardening condition while both slip strains of basal and prismatic <a> decrease with respect to the EQ-hardening condition.

This is followed by discussing changes in the activities of basal and prismatic <a> slip systems. Figs 7 and 8 show that the changes in cumulative slip strains on an average with

respect to the basal and prismatic <a> slip systems within each crystal grain. Fig. 8 shows the rates of increase in both cumulative basal and prismatic <a> slip strains decrease with respect to the cycles for the EQ-hardening condition. In contrast, the cumulative slip strains exhibit a linear increase on the basal slip system for the No-basal hardening condition, and the activity of the basal slip system does not decrease. Fig. 9 shows the dependency of $c^*_{prismatic<a>}$ on the activities of slip systems for the No-basal hardening condition. Increases in the rates of cumulative slip strains on the prismatic <a> slip systems decrease earlier with respect to higher $c^*_{prismatic<a>}$. This is because SSDs are more easily accumulated with higher $c^*_{prismatic<a>}$ as shown in Fig. 10. In contrast, the activity of the basal slip system is higher when $c^*_{prismatic<a>}$ is higher (i.e.,., the activity of the basal slip system is higher in Grain 2 when the work hardening occurs more easily in Grain 1).

In the current simulations, bicrystals are deformed by the forced displacement. The maximum and minimum displacements in the Y-axis remain unchanged throughout the cyclic loading. Additionally, work hardening does not occur in Grain 2 (on the basal slip system) for the No-basal hardening condition. Thus, it is necessary for the activity of the slip system in Grain 2 to remain unchanged throughout the cyclic loading when the Grain 2 is not affected by Grain 1. That is, work hardening of the prismatic <a> slip system in Grain 1 affects the activity of the basal slip system in Grain 2. Therefore, the results indicate that inactivation of the prismatic <a> slip system in a crystal grain potentially activates the slip systems in the neighboring crystal grains.

The activity of the basal slip system decreases for the condition when work hardening occurs in the basal slip system with respect to the EQ-hardening condition, and the trade-off relationship between the activities of slip systems is hidden and could not be recognized. However, the trade-off relationship may result in the scattering of fatigue life, and thus should not be ignored. The mechanisms are discussed in the next section.

3.2 Investigation of effect of incompatibility

Crystal plasticity analysis of unidirectional tensions of bicrystals is performed by employing several CRSSs for the prismatic <a> slip system. Increases in CRSSs for the prismatic <a> slip system stagnate the activity of the prismatic <a>. Thus, work hardening is approximately expressed by increases in CRSSs, and the study investigates the manner in which the work hardening on the prismatic <a> slip system in Grain 1 influences the activity of the basal slip system in Grain 2. The results are shown in Fig. 11.

Fig. 11 shows the distributions of slip strains obtained on the condition PRI-BSL tension. The activity of the prismatic <a> slip system decreases with increases in CRSS for the prismatic <a> slip system while the activity of basal slip system increases. The slip strains are observed within the region near the corner of the bottom in both Grain 1 and 2 and near the grain boundary on the upper side in Grain 2. These results show a tendency similar to those obtained by the current cyclic loading analysis and indicate that similar phenomena are reproduced by the increase in CRSS for the prismatic <a> slip system.

Next, the study examines the results obtained in the condition of PRI-PRI tension in which

the effect of anisotropic elasticity does not appear in the crystal grains in Fig. 12. The prismatic <a> slip system is the primary system in both Grains 1 and 2 for the PRI-PRI tension condition. Two sets of CRSSs are employed, namely one in which the CRSSs of Grain 1 and Grain 2 are equal (EQ-CRSS) and the other in which the CRSSs of Grain 1 exceeds that in Grain 2 (NonEQ-CRSS). In the condition corresponding to EQ-CRSS, the bicrystal deforms homogenously, and the stresses and strains are also homogeneous (Fig. 12 (a), (c)). In condition NonEQ-CRSS, normal stresses in Grain 1 exceed those in Grain 2 (Fig. 12 (b)) while normal strains in the Y-axis are homogeneous (Fig. 12 (c)).

The above homogeneous deformations in the Y-axis indicates that bicrystals deform while maintaining compatibility between Grains 1 and 2. Three reasons are identified with respect to maintaining the compatibility in the condition PRI-PRI tension. First, isotropic elasticity exists within the basal plane. Second, angles of slip plane normal vector and slip direction are 45^{o} with respect to the loading direction (as shown in Fig. 1). The crystal grains maintain the rectangular shapes in both elastic and plastic deformations under the conditions. Third, the bicrystal model is subjected to the forced displacement that is equal between Grains 1 and 2. The difference in the CRSSs between Grains 1 and 2 causes a difference in the elastic and plastic strains in the Y-axis between them. However, the displacements in Grains 1 and 2 are the same in the Y-axis, and the effect of the difference in elastic and plastic strains on inhomogeneous deformation is negligible under the current condition. The elastically compatible-type bicrystals (on the condition corresponding to PRI-PRI tension) deform homogeneously, and thus the elastic incompatibility is mainly attributed to the inhomogeneous deformation on the condition corresponding to PRI-BSL tension and PRI-BSL cyclic conditions.

3.3 Effect of work hardening on activation of slip systems of neighboring crystal grains

It is assumed that the deformation shapes of crystal grains cause the incompatibility. Fig. 13 shows the schematics of deformation shapes of crystal grains when the crystal grains are separated at the grain boundary. In the PRI-BSL condition, Grain 1 with the c-axis corresponding to the Z-axis deforms while maintaining a rectangular shape while Grain 2 with an inclined c-axis deforms with shapes containing shearing (Fig. 13 (a)). Therefore, the gap occurs between Grains 1 and 2 due to the anisotropic elasticity, and Grains 1 and 2 elasto-plastically deform to close the gap. When work hardening occurs in Grain 1, the activity of slip system and deformation volume decrease in Grain 2. The decrease in the deformation volume in Grain 1 must be filled by that in Grain 2. This results in activation of the basal slip system in Grain 2.

Incompatibility in the bicrystal model in the PRI-BSL condition shown in Fig. 13 (a) is treated as a problem of incompatibility around the grain boundary triple junction line when the constrain surface on the top or bottom in the bicrystal model is assumed as the "pseudo" grain boundary. The deformation field formed by the incompatibility around the grain boundary triple junction line contains wedge disclination [33-38]. The deformation field formed by wedge disclination is reproduced by the following procedure shown in Fig. 14: First, a discoidal field is assumed and a wedge-shaped piece is removed from it (Fig. 14 (a)). Second, the discoidal field is deformed such that a newly surface formed by the removal of the piece corresponds to the other surfaces (Fig. 14 (b)).

The deformation field of the wedge disclination is employed to understand

inhomogeneous deformations around grain boundary triple junction lines. Kondou & Ohashi [33,35] conducted uniaxial tensile analysis using symmetric and asymmetric bicrystal models. They suggested that inhomogeneous deformation fields in the bicrystals induced by the boundary conditions and plastic anisotropy corresponded to those by the disclination. The factors contributing to developments of geometrically necessary dislocation (GND) bands formed in the bicrystal [33,35] and tricrystal models [36] were explained using the disclination-type deformation field. Hosoya et al. [37] and Hosoya [38] proposed finite element methods in solids with disclination and applied them to elastic incompatibility problems in tricrystals. This included investigating the accuracy. The results showed that stress fields around the grain boundary triple junction lines were approximately reproduced by using crystal grains with isotropic elasticity and disclination.

The trade-off relationship of slip systems between Grains 1 and 2 in the PRI-BSL condition is explained (Fig. 11) by employing a field of the wedge disclination-type deformation. Slip systems are activated within larger regions near the bottom than those near the top in the bicrystal model. The work hardening around the grain boundary triple junction line on the bottom surface mainly affects the deformation field when compared to that around the grain boundary triple junction line on the top surface. Thus, the changes in deformation field around the grain boundary triple junction line on the bottom are investigated. The deformation field around the grain boundary triple junction line on the bottom is expressed by the wedge disclination-type deformation as shown in Fig. 15. The new surfaces that are produced by the removal of the wedge piece from the disc correspond to the grain boundary and the region of left-hand side of the disc (denoted as Grain 1) and the right-hand side (denoted as Grain 2). The bottom interface of Grains 1

and 2 is subjected to the restraint of deformation in the Y-direction.

The gap resulting from anisotropic elasticity (Fig. 15 (a)) is closed by the elasto-plastic deformations of Grains 1 and 2 (Fig. 15 (b)). In the No-basal hardening condition, work hardening occurs only in Grain 1 under a cyclic loading, and the volume of plastic deformation decreases in Grain 1. In order to ensure the boundary in Grain 1 conforms to that in Grain 2, it is necessary to compensate the decrease in deformation volume in Grain 1 by the increase in that in Grain 2 (Fig. 15 (c)). Thus, the inactivation of slip system by work hardening in Grain 1 leads to the increase of deformation volume (i.e.,., the activation of slip systems) in Grain 2. The results suggest the possibility that the activity of basal slip system increases in the neighboring crystal grains arranged even in the direction perpendicular to the loading direction when the activity of prismatic <a> slip system increases in the crystal grains.

3.4 Effect of boundary condition on the activities of slip systems

Effects of the boundary conditions in the bicrystals are investigated by using tricrystal models (Fig. 4) in which the third crystal grain sets are on the top (Tricrystal A) or bottom of the bicrystal (Tricrystal B). The conditions of the analysis are similar to those of the bicrystal model with the BSL-PRI tension condition, and several CRSSs for the prismatic <a> slip system in Grain 1 are employed as shown in Table 3. The results are shown in Figs. 16 and 17.

Fig. 16 shows the results obtained by employing model Tricrystal A (Fig. 4 (a)). The

distributions of slip strains on prismatic <a> and basal slip systems indicate that the prismatic <a> slip system in Grain 1 and the basal slip system in Grain 2 are activated depending on their crystal orientations. All slip systems are not activated in Grain 3 since Schmid factors for the basal and prismatic <a> slip systems correspond to zero. The localized slip strains occur within the region near the corner in the bottom side in Grain 1 and near the grain boundary in Grain 2. The tendency is similar to the results obtained by the bicrystal model with the BSL-PRI tension condition while the slip systems are activated in the regions larger than those of the bicrystal model.

Next, the dependency of activity of the basal slip system on the CRSSs for the prismatic <a> slip system is observed as shown in Fig. 16. The tendency corresponds with the result obtained in the BSL-PRI tension condition in Fig. 11. The trade-off in the relationship of activities between basal and prismatic <a> slip systems is observed. Thus, the boundary condition does not significantly influence on the activity of slip systems in the Tricrystal A condition.

Fig. 17 shows the results obtained in the Tricrystal B condition, and the regions where the basal slip system activates near the grain boundary and the corner in the bottom side in Grain 2. The tendency is the same as that of Tricrystal A. However, distributions of the slip strain and the dependency of the activities of slip systems on CRSSs for the prismatic <a> in Tricrystal A condition differ substantially from those for Tricrystal B condition. The prismatic <a> slip system that activates within the whole region in Grain 1 does not include the region around the boundary triple junction line, and it is not possible to directly observe localized slip strains at the corner in Grain 1. The dependency of

activities of slip systems on the CRSSs for the prismatic <a> does not suggest a trade-off relationship. Both activities of prismatic <a> and basal slip systems decrease with increasing in the CRSSs for the prismatic <a>.

We examine the reason for the differences between the results obtained in the Tricrystal A and B conditions by employing the deformation field of disclination as shown in Fig. 18. In contrast to the results obtained for the Tricrystal A condition, the gap between Grain 1 and 2 is closed by the deformation of Grain 3 as well as those of Grains 1 and 2 in the Tricrystal B condition. The deformation of Grain 3 decreases the deformation volumes of Grains 1 and 2, and the plastic deformation does not exist around the grain boundary triple junction line in the current condition. Within the elastic regions, changes in CRSSs for the prismatic <a> slip system do not influence the activities of slip systems. Therefore, an increase of CRSSs for the prismatic <a> slip system does not affect the deformation field of disclination on the current condition since the elastic deformation occurs around the grain boundary triple junction line without plastic deformation. The activity of the basal slip system is not changed by changes of CRSSs for the prismatic <a>. These results indicate that a potential exists for changes in which slip systems activate and work hardening exists depending on the boundary conditions, and the effect of the work hardening on the activation of slip systems also changes based on the locations in which work hardening exists.

3.5 Effects of work hardening with respect to the regions

The trade-off in the relationship of activities of basal and prismatic <a> slip systems is

examined by considering the wedge disclination-type deformation field: the prismatic <a> slip system is first activated and then work hardening occurs around the grain boundary triple junction line. The decrease in the prismatic <a> slip affects the disclination-type deformation field. This may result in activation of basal slip systems. However, the disclination-type deformation cannot be used to explain the decrease of the activity of basal slip system with decreases in that of prismatic <a> slip (Fig. 17).

Wedge disclination-type deformation fields are formed by wedge-shaped incompatibility around the grain boundary triple junction lines. Thus, incompatibility of normal strains in the loading direction is not considered in the wedge disclination. As shown in Fig. 19, incompatibility exists between Grains 1 and 2 in the loading direction due to anisotropic elasticity and difference in CRSSs for the primary slip systems in Grains 1 and 2 when a difference in the displacements is allowed in the loading direction between Grains 1 and 2. The occurrence of work hardening and reduction of deformation volume in Grain 1 under cyclic loading prevents deformation of Grain 2 in the Y-axis. This is due to Grain 1 since Grain 2 shares the grain boundary with Grain 1. Hence, it is necessary for Grains 1 and 2 to deform to conform the grain boundary with the other. Therefore, the effect of work hardening in Grain 1 is stronger in the region nearer the grain boundary. Thus, a decrease in activity in prismatic <a> slip system in Grain 1 can decrease the activity of the basal slip system near the grain boundary in Grain 2.

Macroscopic displacements are unchanged with respect to the condition of forced displacements, and it is necessary to directly offset a decline in the deformation volumes of crystal grains in the loading direction with respect to increasing volumes of the other

crystal grains arranged in the loading direction. Specifically, normal strains in Y-axis in Grain 3 increase with decreases in those in Grain 1 as shown in Figs. 16 and 17. Given the condition that Grain 3 has a crystal orientation in which slip systems are activated, the activities of slip systems in Grain 3 increase with decreasing the deformation volumes in Grains 1 and 2. However, sufficient results were obtained in the study to explain this type of a relationship between strain redistribution and activation of slip systems in the loading direction, and thus additional investigations are required.

In this study, the results indicate that incompatibility derived from anisotropic elasticity and its changes by work hardening on the prismatic <a> slip system activate the basal slip system in the arranged neighboring crystal grains even in the direction perpendicular to the loading direction. The result reveals the basal slip system in the neighboring crystal grains is activated with decreases in the activity of prismatic <a> slips by the work hardening under a fatigue loading although the prismatic <a> slips initially operate in a crystal grain.

It is barely possible to detect the effect of wedge disclination-type incompatibility and work hardening on activities of slip systems especially in the condition that crystal grains arranged in a direction perpendicular to the loading direction. This is because the effect did not appear on the condition in which work hardening existed on the basal slip system (EQ-hardening condition) as shown in Fig. 8 and in the condition that work hardening did not occur around the triple junction line (i.e.,., on the condition that work hardening did not occur within the regions that are directly relevant to the formation of the disclination-type deformation fields) as shown in Fig. 17. However, factors, such as the minute

changes of activities of slip systems may affect the fatigue mechanisms and result in scattering with respect to the fatigue life in the HCF or VHCF regime.

4 Conclusions

In this study, the following analyses were performed: (i) cyclic loading plasticity analysis employing a bicrystal model, and (ii) uniaxial tensile loading analysis employing bicrystal and tricrystal models. Additionally, the study investigated the effect of changes in incompatibility by work hardening on the activity of basal slip system in the α phase of Ti-6Al-4V alloy. The results can be summarized as follows;

1) Incompatibility between crystal grains derived from anisotropic elasticity was weakened by the deformations of elasto-plastic deformations. Thus, the occurrence of work hardening in a crystal grain decreases the volume of deformation and increase those of elasto-plastic deformations increases in neighboring crystal grains. The phenomenon leads to activation of slip systems in neighboring crystal grains. Thus, although the prismatic <a> slips initially operates under cyclic loading, the basal slip system in the neighboring crystal grains displays a potential for activation by work hardening on the prismatic <a> slip system.

2) It is assumed that the surfaces subjected to the displacement restraint in the bicrystal model correspond to pseudo grain boundaries. Therefore, the lines in which the actual grain boundary and pseudo grain boundary intersect are considered as boundary triple junction lines. The deformation field around the boundary triple junction line is easily determined by using a wedge disclination-type deformation field and this also helps in understanding changes in incompatibility with work hardening around the triple junction line.

3) The effects of work hardening on the activities of slip systems were changed depending on the locations where the work hardening occurred. Activities of slip systems of neighboring crystal grains were increased when work hardening occurred within the regions around the triple junction line involved in formation of wedge disclination-type deformation field. Conversely, the activities of slip systems were decreased in the neighboring crystal grains arranged in the direction perpendicular to the loading direction when work hardening occurred to prevent the deformation in the loading direction in a crystal grain.

Acknowledgement

This work was partly supported by Council for Science, Technology and Innovation (CSTI), Cross-ministerial Strategic Innovation Promotion Program (SIP), "Fundamental Research Focusing on Interface for Overcoming Unsolved Issues in Structural Materials" (Founding agency: JST). Mr. Kenta Nyui and Mr. Morihiro Sakamoto graduated from Advanced Course of Production System Engineering, National Institute of Technology, Asahikawa College, are acknowledged for this helpful discussion.

References

[1] Welsch G, Boyer R. Collings E.W. (Eds.) Materials properties handbook: Titanium Alloys. ASM International 1994.

[2] Pederson R. Microstructure and phase transformation of Ti-6Al-4V. Licentiate thesis, Luleå university of technology 2002. doi:LTU-LIC-0230-SE.

[3] Le Biavant K, Pommier S, Prioul C. Local texture and fatigue crack initiation in a Ti-6Al-4V titanium alloy. Fatigue Fract Eng Mater Struct 2002;25:527–45. doi:10.1046/j.1460-2695.2002.00480.x.

[4] Bantounas I, Dye D, Lindley TC. The role of microtexture on the faceted fracture morphology in Ti–6Al–4V subjected to high-cycle fatigue. Acta Mater 2010;58:3908–18. doi:10.1016/j.actamat.2010.03.036.

[5] Dunne FPE, Walker A, Rugg D. A systematic study of hcp crystal orientation and morphology effects in polycrystal deformation and fatigue. Proc R Soc London A Math Phys Eng Sci 2007;463:1467–89. doi:10.1098/rspa.2007.1833.

[6] Bantounas I, Dye D, Lindley TC. The effect of grain orientation on fracture morphology during high-cycle fatigue of Ti–6Al–4V. Acta Mater 2009;57:3584–95. doi:10.1016/j.actamat.2009.04.018.

[7] Ishihara S, Mcevily AJ. On the Early Initiation of Fatigue Cracks in the High Cycle Regime. Proc ICF 2009;12:12-7.

[8] McDowell DL, Dunne FPE. Microstructure-sensitive computational modeling of fatigue crack formation. Int J Fatigue 2010;32:1521–42. doi:10.1016/j.ijfatigue.2010.01.003.

[9] Bridier F, Villechaise P, Mendez J. Analysis of the different slip systems activated by tension in a α/β titanium alloy in relation with local crystallographic orientation. Acta Mater 2005;53:555–67. doi:10.1016/j.actamat.2004.09.040.

[10]Mayeur JR, McDowell DL. A three-dimensional crystal plasticity model for duplex Ti–6Al–4V. Int J Plast 2007;23:1457–85. doi:10.1016/j.ijplas.2006.11.006.

[11] Medina Perilla JA., Gil Sevillano J. Two-dimensional sections of the yield locus of a Ti-6%Al-4%V alloy with a strong transverse-type crystallographic α-texture. Mater Sci Eng A 1995;201:103–10. doi:10.1016/0921-5093(95)09780-5.

[12] Semiatin SL, Bieler TR. Effect of texture and slip mode on the anisotropy of plastic flow and flow softening during hot working of Ti-6Al-4V. Metall Mater Trans A Phys Metall Mater Sci 2001;32:1787–99. doi:10.1007/s11661-001-0155-1.

[13] Bridier F, McDowell DL, Villechaise P, Mendez J. Crystal plasticity modeling of slip activity in Ti-6Al-4V under high cycle fatigue loading. Int J Plast 2009;25:1066–82. doi:10.1016/j.ijplas.2008.08.004.

[14] Inoko F. Deformation and fatigue in bicrystals. J Japan Inst Light Met (in Japanese) 1980;30:512–9.
[15] Osterstock S, Robertson CF, Sauzay M, Degallaix S, Aubin V. Prediction of the Scatter of Crack Initiation under High Cycle Fatigue. Key Eng Mater 2007;345–346:363–6. doi:10.4028/www.scientific.net/KEM.345-346.363.
[16] Kang DS, Lee KJ, Kwon EP, Tsuchiyama T, Takaki S. Variation of work hardening rate by oxygen contents in pure titanium alloy. Mater Sci Eng A 2015;632:120–6. doi:10.1016/j.msea.2015.02.074.
[17] Hook RE, Hirth, JP. The deformation behavior of isoaxial bicrystals of Fe-3%Si. Acta Metallurgica 1967;15:535-51. doi:10.1016/0001-6160(67)90087-9.
[18] Hook RE, Hirth JP. The deformation behavior of non-isoaxial bicrystals of Fe-3%Si. Acta Metall 1967;15:1099–110. doi:10.1016/0001-6160(67)90383-5.
[19]Spearot DE, Jacob KI, McDowell DL. Nucleation of dislocations from [0 0 1] bicrystal interfaces in aluminum. Acta Mater 2005;53:3579–89. doi:10.1016/j.actamat.2005.04.012.
[20]Shibutani Y, Hirouchi T, Tsuru T. Transfer and Incorporation of Dislocations to Sigma3 Tilt Grain Boundaries under Uniaxial Compression. J Solid Mech Mater Eng 2013;7:571–84. doi:10.1299/jmmp.7.571.
[21]Ohashi T. Computer simulation of non-uniform multiple slip in face centered cubic bycrystals. Trans Japan Inst Met 1987;28:906–15.
[22]Ma A, Roters F, Raabe D. A dislocation density based constitutive law for BCC materials in crystal plasticity FEM. Comput Mater Sci 2007;39:91–5. doi:10.1016/j.commatsci.2006.04.014.
[23] Kondou R, Ohashi T. Crystal plasticity analysis of non-uniform deformation in symmetric type bicrystals under tensile load and formation of geometrically necessary dislocation bands. J Solid Mech Mater Eng (in Japanese) 2007;1:114–25. doi:10.1299/jmmp.1.114.
[24] Mayama T, Ohashi T, Kondou R. Geometrically necessary dislocation structure organization in FCC bicrystal subjected to cyclic plasticity. Int J Plast 2009;25:2122–40. doi:10.1016/j.ijplas.2009.02.001.
[25] Kawano Y, Tamaru N, Ishii S, Mayama T, Kondou R, Ohashi T. Grain boundary inclination dependence of GN dislocation patterns and density in bicrystal model. Trans JSME (in Japanese) 2015;81:1-14. doi:10.1299/transjsme.14-00630.
[26]Ohashi T, Kondou R. Evolution of dislocation patterns in a tricrystal model subjected to cyclic loading. Philos Mag 2013;93:366–87. doi:10.1080/14786435.2012.721017.
[27] Ohashi T. Numerical modelling of plastic multislip in metal crystals of f.c.c. type.

Philos Mag A 1994;70:793–803.
[28] Hill R., Generalized constitutive relations for incremental deformation of metal crystals by multislip. J Mech Phys Solids 1966;14:95-102. doi:10.1016/0022-5096(66)90040-8.
[29]Castelluccio GM, McDowell DL. Mesoscale cyclic crystal plasticity with dislocation substructures. Int J Plast 2017:1–26. doi:10.1016/j.ijplas.2017.06.002.
[30] Kuroda M, Tvergaard V. On the formulations of higher-order strain gradient crystal plasticity models. J Mech Phys Solids 2008;56:1591–608. doi:10.1016/j.jmps.2007.07.015.
[31]Fisher ES, Renken CJ. Single-crystal elastic moduli and the hcp → bcc transformation in Ti, Zr, and Hf. Phys Rev 1964;135:A482–94. doi:10.1103/PhysRev.135.A482.
[32] Bache MR. A review of dwell sensitive fatigue in titanium alloys: the role of microstructure, texture and operating conditions. Int J Fatigue 2003;25:1079–87. doi:10.1016/S0142-1123(03)00145-2.
[33]Kondou R, Ohashi T. Grain boundary accumulation of geometrically necessary dislocation and asymmetric deformation in compatible-type bicrystals with tilt angle grain boundary under tensile loading. Trans Japan Soc Mech Eng Ser A 2006;72:16–23. doi:10.1299/kikaia.72.16.
[34] Volterra V. Sur l'equilibre des corps elastiques multiplement connexes. Ann Ec Norm (Paris) 1907;24:401–517.
[35] Kondou R, Ohashi T, Miura S. Relationship between Micro-Incompatibility and Heterogeneity of Dislocation Density Distribution in Cu-9at.% Al Symmetric Type Bicrystal Models under Tensile Loading. J Comput Sci Technol 2008;2:162–72 (in Japanese). doi:10.1299/jcst.2.162.
[36] Kondou R, Ohashi T. Multi-Body Interaction of Crystal Grains in Compatible-Type Tricrystals under Tensile Loading and Formation of Disclination-Type Displacement Field. J Environ Eng 2008;3:295–306. doi:10.1299/jee.3.295.
[37] Hosoya T, Katoh, Sasaki K. Finite element models of wedge disclination. Trans JSME (in Japanese) 2014;80:1-12. doi:10.1299/transjsme.2014smm0313.
[38] Hosoya T. Finite element method in solid with disclination and its application to elastic incompatibility problem. Doctoral theses, Hokkaido univ (in Japanese) 2015.

Figures

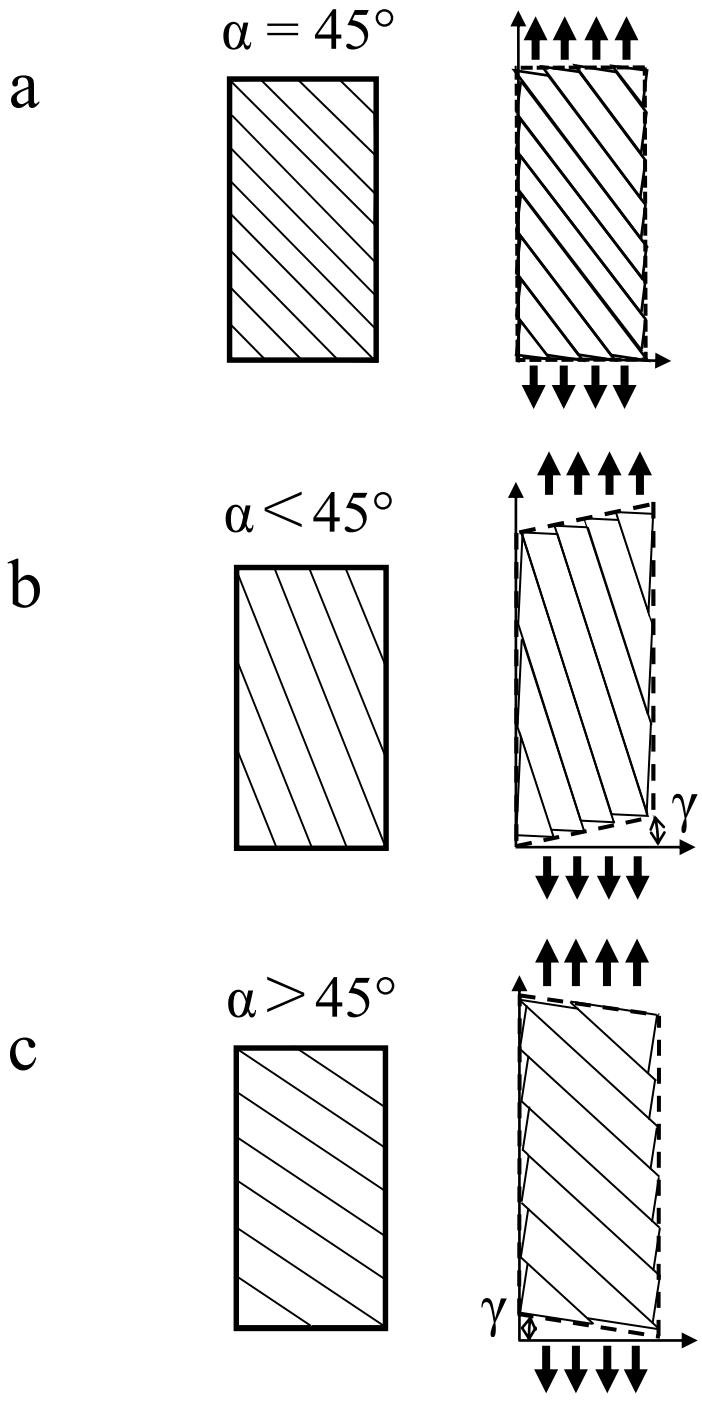

Fig. 1 Deformation shapes of single crystals based on angles of slip planes to the loading direction where a denotes the angle between the slip plane and loading direction.

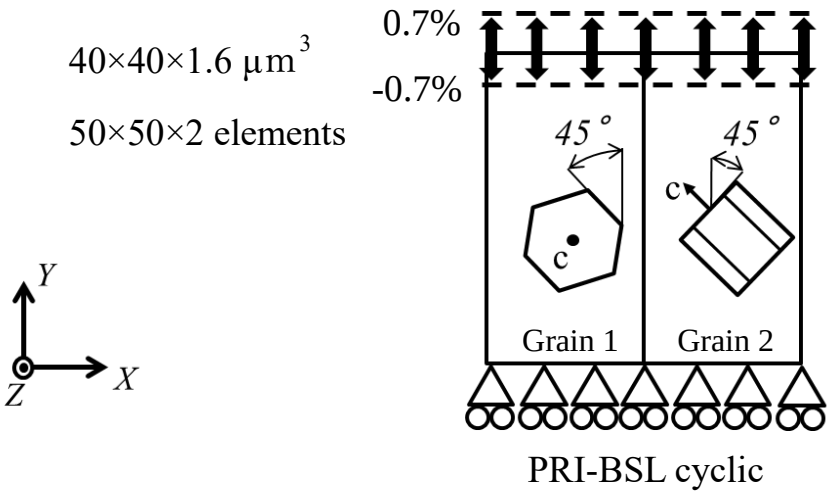

Fig. 2 Schematic of the analysis model and boundary conditions for cyclic loading analysis.

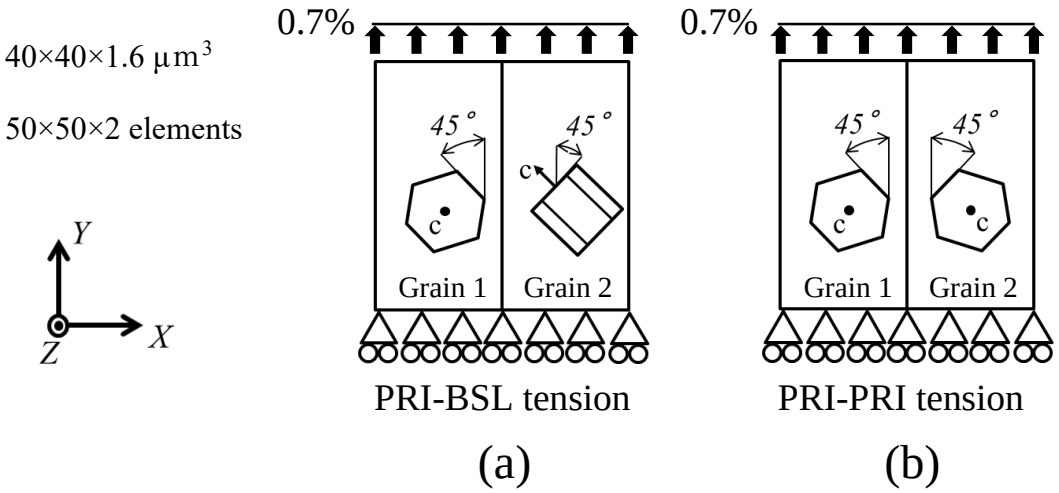

Fig. 3 Schematic of the analysis model and boundary conditions for uniaxial loading analysis of bicrystals.

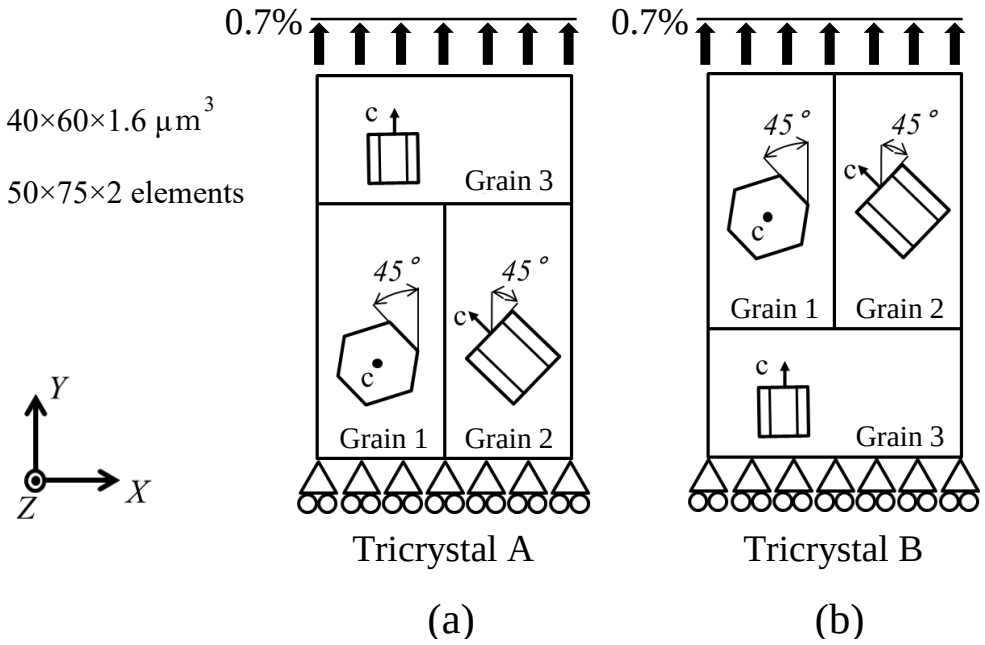

Fig. 4 Schematic of the analysis model and boundary conditions for uniaxial loading analysis of tricrystals.

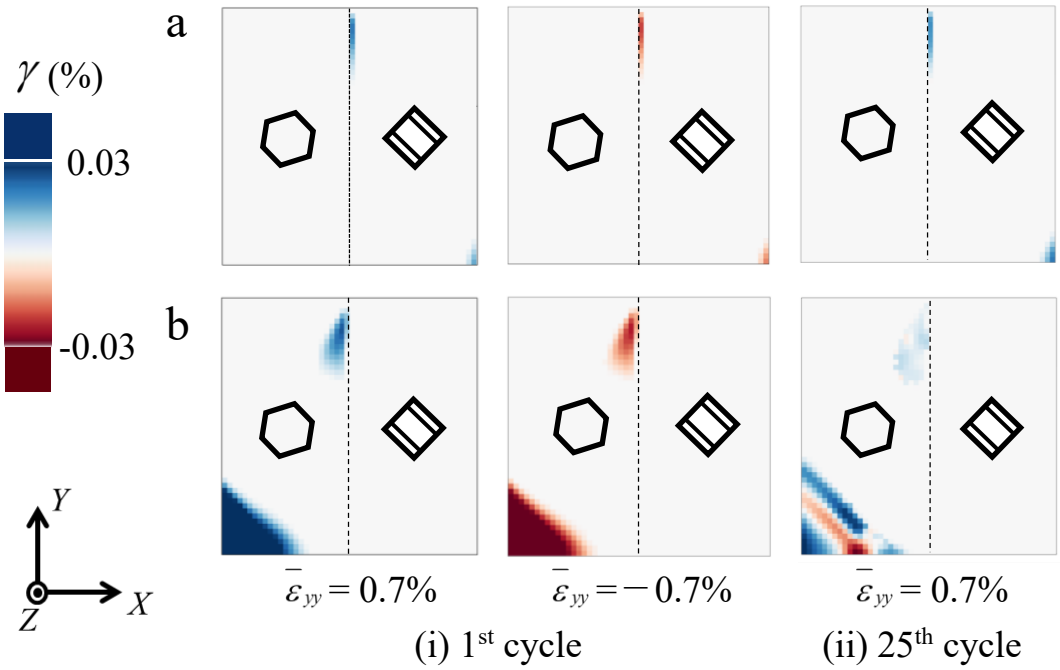

Fig. 5 Distributions of slip strains on the basal (a) and prismatic <a> slip system (b) during cyclic loading at (i) the 1st peak strain of tension and compression and (ii) the 25th peak strain of tension. The No-basal hardening condition is employed and $c^*_{prismatic<a>} = 15.0$.

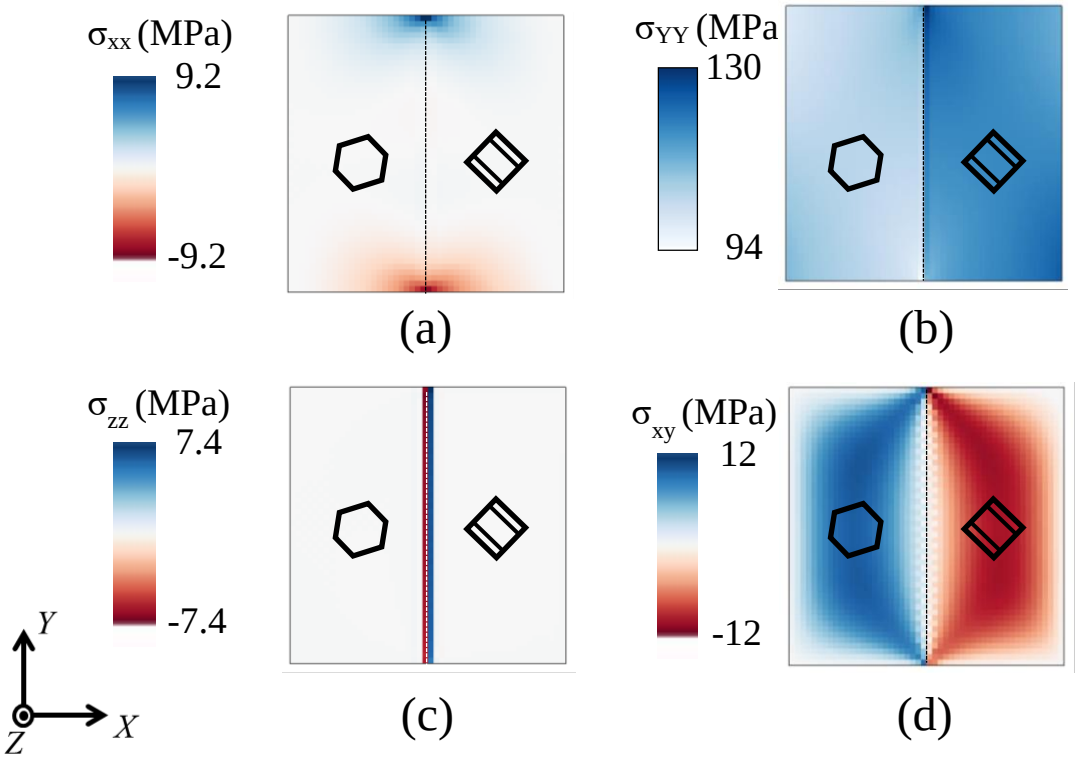

Fig. 6 Distributions of stresses at the elastic stage ($\bar{\varepsilon}_{YY}$ = 0.1%): (a) normal stress in the X-axis, (b) in the Y-axis, and (c) in the Z-axis, and (d) X-Y component of shear stress.

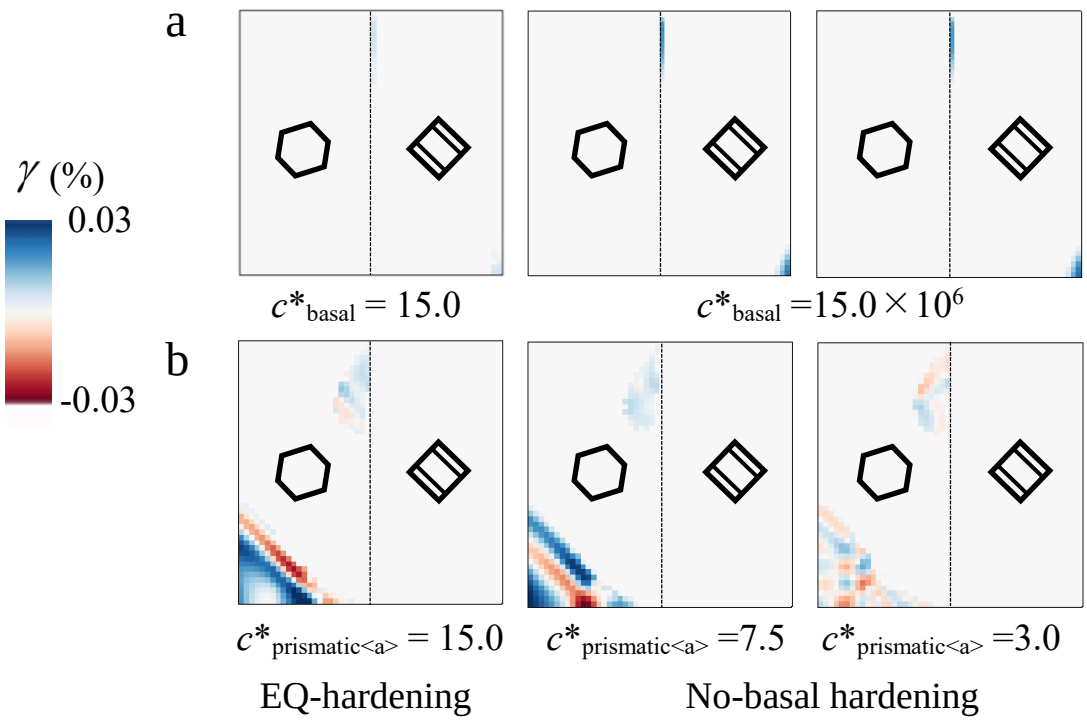

Fig. 7 Effect of c^* on the distributions of slip strains on the basal (a) and prismatic <a> slip system (b) at the 25th peak strain of tension.

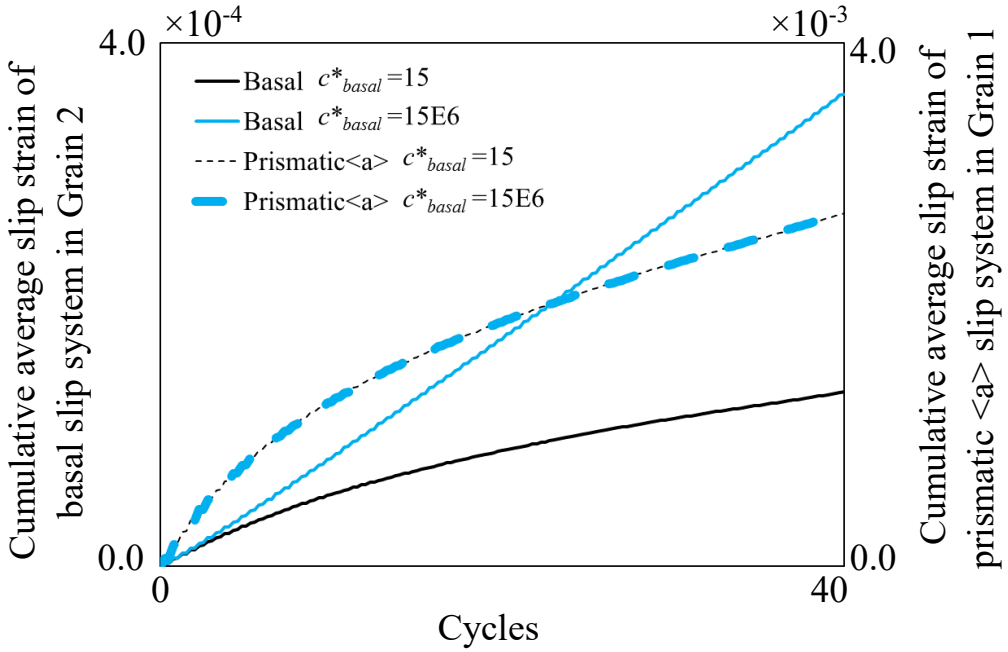

Fig. 8 Difference in cumulative slip strains between EQ-hardening and No-basal hardening conditions in which $c^*_{prismatic<a>}$ corresponds to 15.0 throughout the series of simulations.

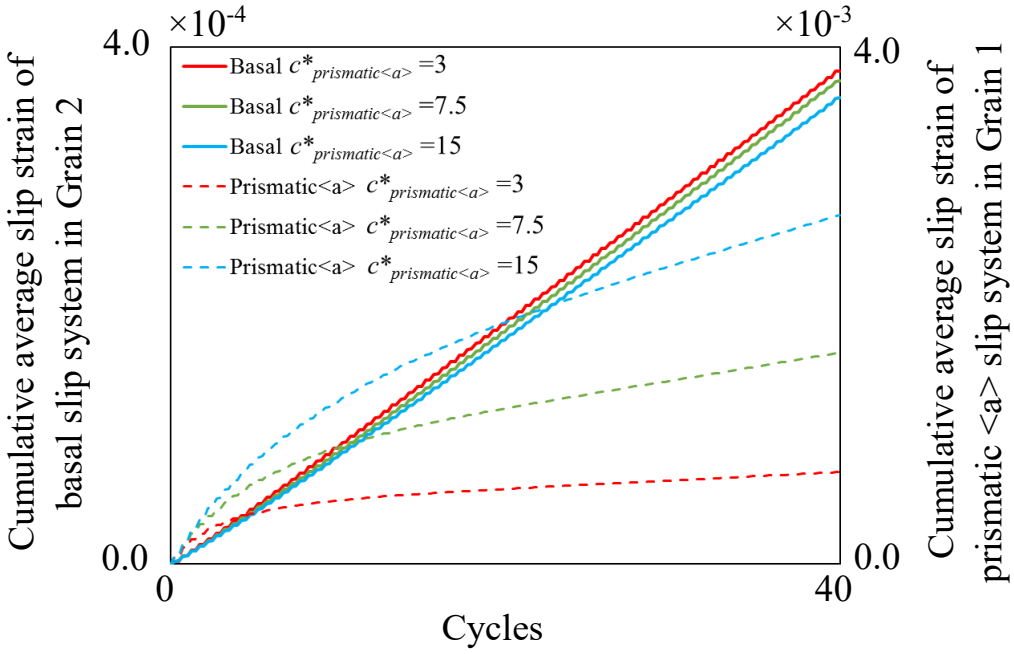

Fig. 9 Activity changes in slip systems based on $c^*_{prismatic<a>}$ with respect to the No-basal hardening condition where c^*_{basal} corresponds to 15.0×10^6 throughout the series of simulations.

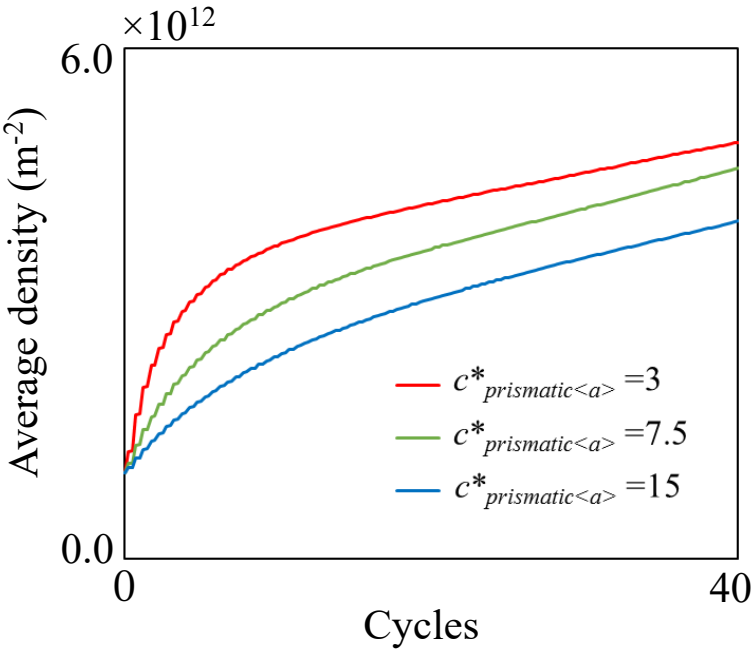

Fig. 10 Average SSD densities of the prismatic slip system in Grain 1 based on $c^*_{prismatic<a>}$.

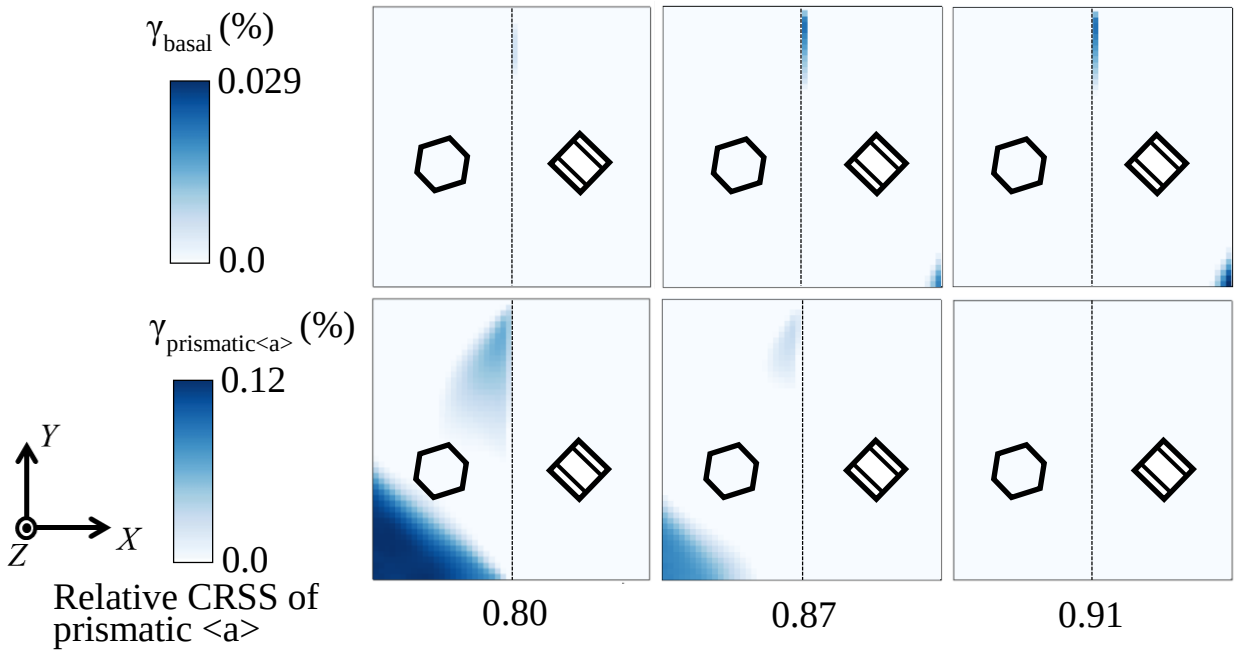

Fig. 11 Distributions of slip strains based on relative CRSSs for the prismatic <a> slip system normalized to those for the basal slip system.

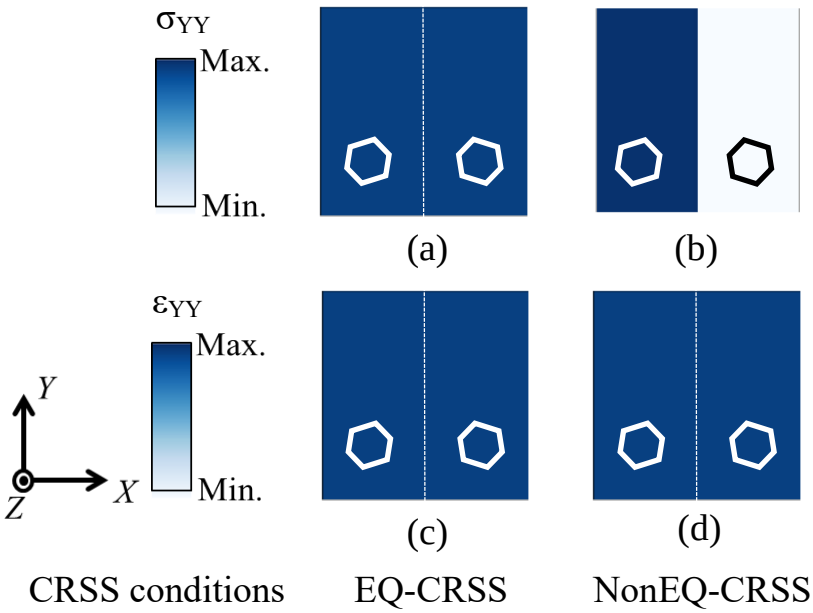

Fig. 12 Distributions of normal stress σ_{YY} and normal strain ε_{YY} in the model PRI-PRI tension. (a) σ_{YY} in the EQ-CRSS condition, (b) σ_{YY} in the NonEQ-CRSS condition, (c) ε_{YY} in the EQ-CRSS condition, and (d) ε_{YY} in the NonEQ-CRSS condition.

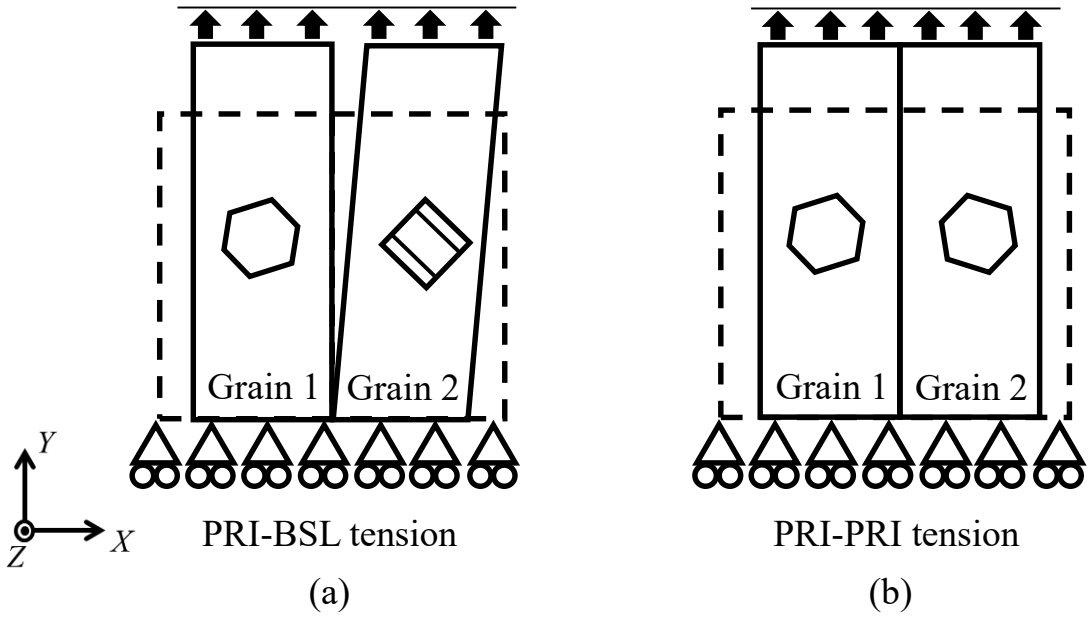

Fig. 13 Schematic of deformed shapes of crystal grains in which the crystal grains are separated at the grain boundaries.

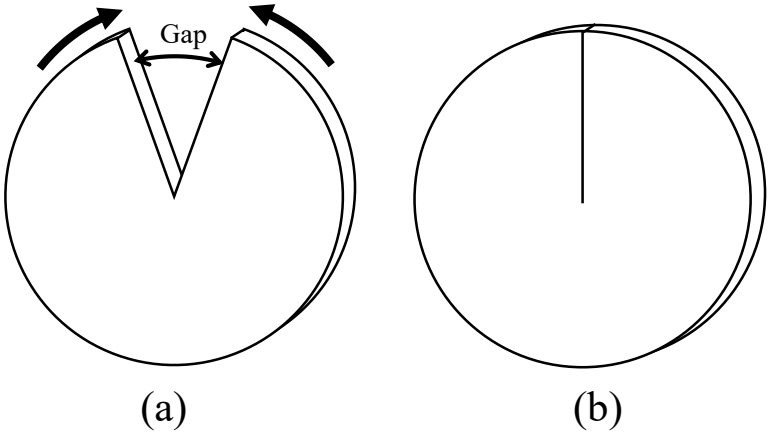

Fig. 14 Wedge disclination type deformation. States (a) before and (b) after jointing the boundary.

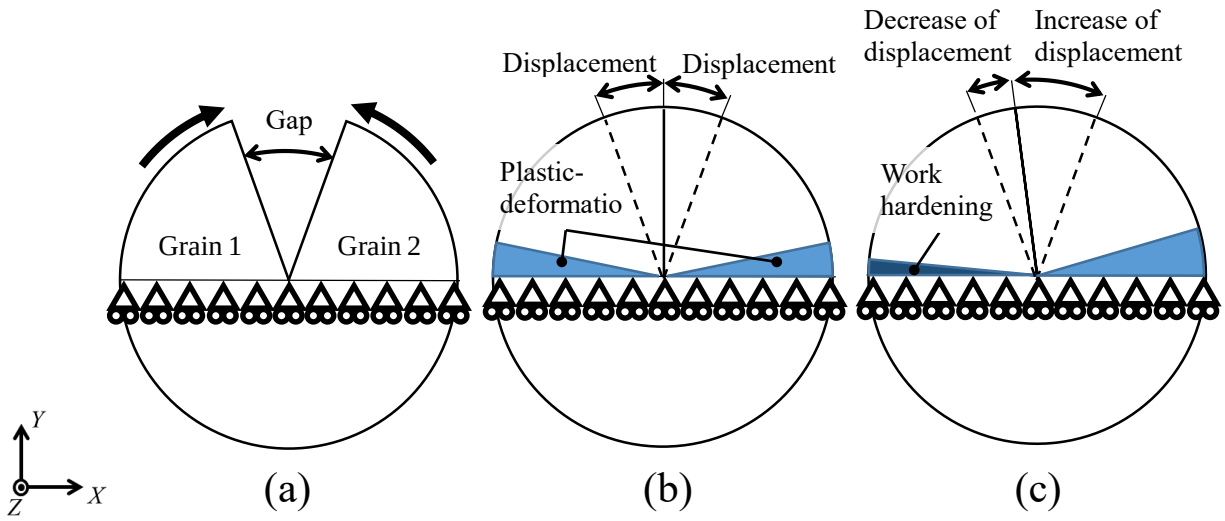

Fig. 15 Schematics showing the (a) initial condition and (b) wedge disclination type deformation before and (c) after work hardening.

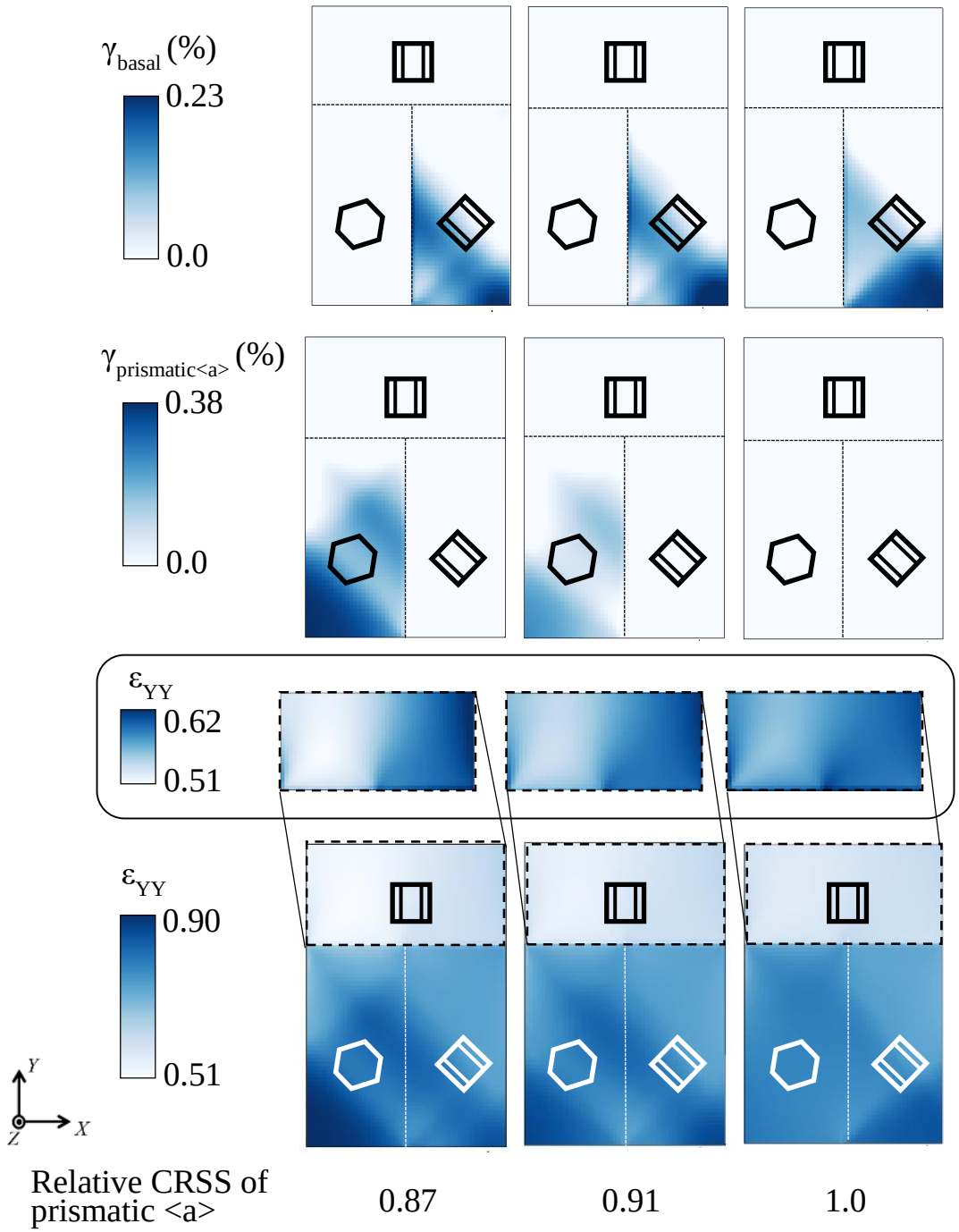

Fig. 16 Distributions of slip strains on the basal and prismatic <a> slip systems and normal strains in the Y-axis when another crystal grain arranged on the top of the bicrystal model. $\bar{\varepsilon}_{yy}$ = 0.7 %.

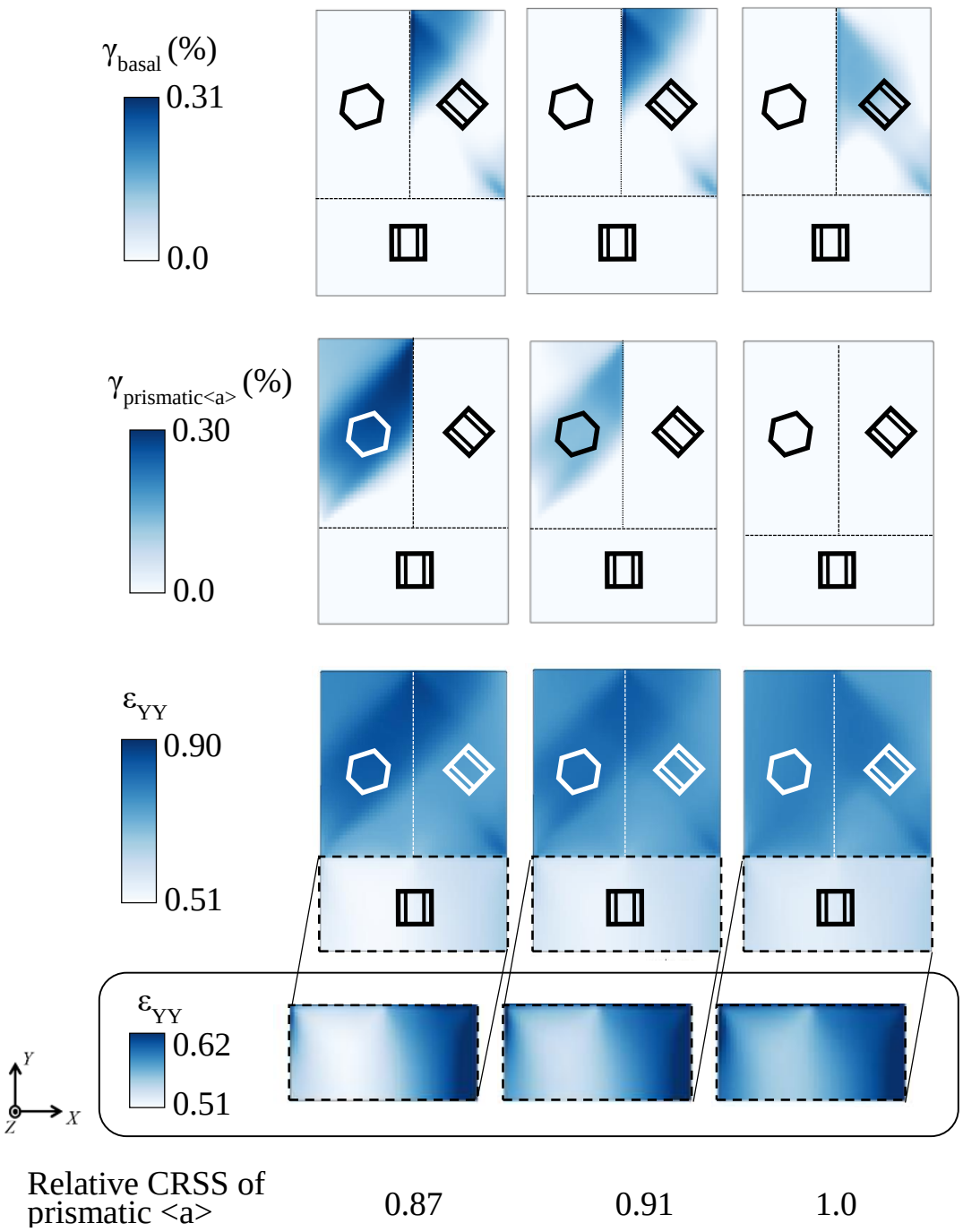

Fig. 17 Distributions of slip strains on the basal and prismatic <a> slip systems and normal strains in the Y-axis when another crystal grain arranged on the bottom of the bicrystal model. $\bar{\varepsilon}_{yy}$ = 0.7 %.

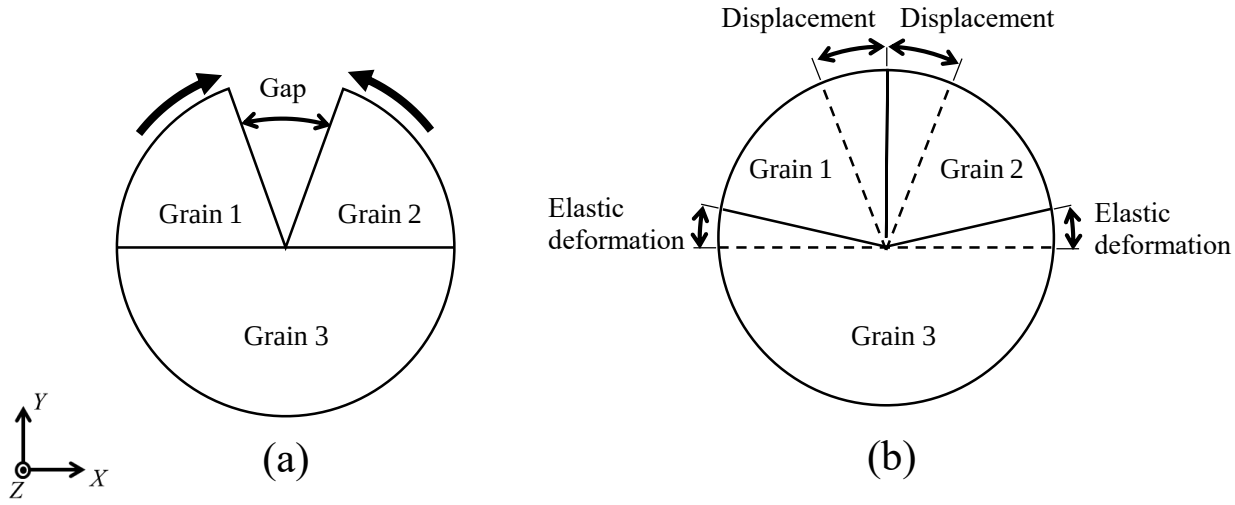

Fig. 18 Schematics showing (a) incompatibility between crystal grains and (b) closing of the gap due to wedge disclination-type deformation.

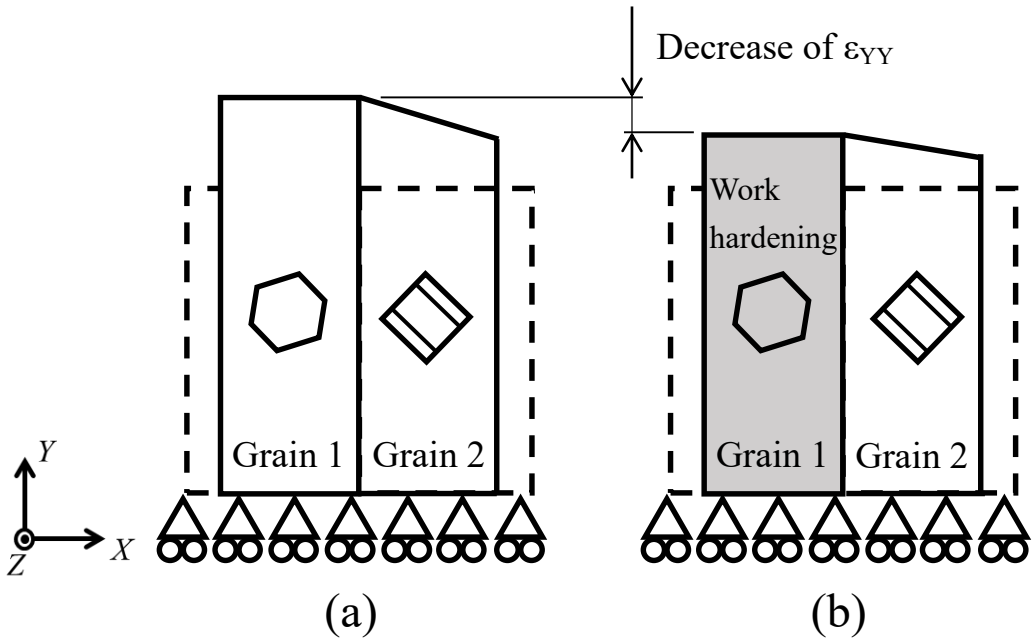

Fig. 19 Schematics showing the decrease in the deformation volume of the bicrystal in Y-axis due to work hardening under the condition in which uniform stress is virtually applied to the top surface. The states (a) before and (b) after work hardening.

Tables

Table 1 Elastic compliances for Ti with an hcp structure [$(TPa)^{-1}$] [31].

S_{11}	S_{12}	S_{13}	S_{33}	S_{44}
9.581	-4.623	-1.893	6.980	21.413

Table 2 c^* for cyclic loading analysis.

Slip systems	EQ-hardening	No-basal hardening
c^*_{basal}	15.0	15.0×10^6
$c^*_{prismatic<a>}$		3.0 7.5 15.0

Table 3 The initial CRSS for each slip system, relative CRSS of basal slip system normalized to CRSS for the prismatic <a> slips, and relative CRSS of prismatic <a> slip system normalized to CRSS for the basal slips.

	PRI-BSL cyclic	PRI-BSL tension	Tricrystal A Tricrystal B
CRSS of basal	425.5 MPa		
CRSS of prismatic <a>	370.0 MPa	340.4 – 444.0 MPa	370.0 – 444.0 MPa
Relative CRSS of basal	1.15	0.96 – 1.25	0.96 – 1.15
Relative CRSS of prismatic <a>	0.870	0.800 – 1.04	0.870 – 1.04

Table 4 The initial CRSSs for the prismatic <a> slip system employed in the PRI-PRI tension analysis [MPa].

	EQ-CRSS	NonEQ-CRSS
Grain 1	370.0	370.0
Grain 2	370.0	444.0